Journal of Geophysical Research: Atmospheres

RESEARCH ARTICLE
10.1029/2018JD028605

# Last Glacial Maximum and Mid-Holocene Thermal Growing Season Simulations

**Dabang Jiang**[1,2,4,5], **Yue Sui**[3], **Xianmei Lang**[1,4,5], **and Zhiping Tian**[1,5]

[1]Institute of Atmospheric Physics, Chinese Academy of Sciences, Beijing, China, [2]School of Environmental Studies, University of Chinese Academy of Sciences, Beijing, China, [3]Department of Atmospheric Science, School of Environmental Studies, China University of Geosciences, Wuhan, China, [4]Collaborative Innovation Center on Forecast and Evaluation of Meteorological Disasters, Nanjing University of Information Science and Technology, Nanjing, China, [5]CAS Center for Excellence in Tibetan Plateau Earth Sciences, Beijing, China

**Key Points:**
- We present a simulation analysis of the last glacial maximum and mid-Holocene growing season changes relative to preindustrial levels
- There is a shortening of the growing season and a decrease of the growing degree days above 5 °C at the last glacial maximum
- The mid-Holocene growing season resembled preindustrial states globally but featured a latitude-varying difference

**Supporting Information:**
- Supporting Information S1

**Correspondence to:**
D. Jiang,
jiangdb@mail.iap.ac.cn

**Citation:**
Jiang, D., Sui, Y., Lang, X., & Tian, Z. (2018). Last glacial maximum and mid-Holocene thermal growing season simulations. *Journal of Geophysical Research: Atmospheres*, *123*, 11,466–11,478. https://doi.org/10.1029/2018JD028605

Received 1 MAR 2018
Accepted 2 OCT 2018
Accepted article online 12 OCT 2018
Published online 29 OCT 2018



**Abstract** The growing season—the number of days per year during which the climate favors plant growth—is an important factor for describing climate. Based on daily data of all available numerical experiments from the Paleoclimate Modeling Intercomparison Project phases two and three, we examine the growing season over global ice-free land for the last glacial maximum and mid-Holocene to improve our understanding of glacial and interglacial climates. Compared to the preindustrial period, the last glacial maximum growing season was shortened at midlatitude and high latitude and by 26.1 days globally in terms of nine climate models due to a later start and an earlier end. Growing degree days above 5 °C (GDD5) decreased by 24% due to both cooling and shortening of the growing season, agreeing with pollen-based reconstructions of globally decreased signal and spatial pattern of GDD5 changes at 88 grid cells. Twenty-four models indicate that the mid-Holocene growing season start and end dates and length were similar to preindustrial states globally but featured a latitude-varying difference. The length increased north of ~50°N and decreased in much of the area from 20–50°N owing to variations in both the start and end dates. In response to orbital forcing, both the growing season temperature and GDD5 increased at northern midlatitude and high latitude but decreased elsewhere. The GDD5 simulations agreed in sign with the reconstructions at 516 grid cells more often than not, though their spatial patterns were different to some extent.

## 1. Introduction

The last glacial maximum (LGM, ca. 21,000 years ago) and mid-Holocene (ca. 6,000 years ago) are two important periods for understanding past glacial and interglacial environments. The former period represents a typical interval during which global volumes of ice sheets and atmospheric greenhouse gases were, respectively, at their highest and lowest levels over the last glacial period. The latter period, on the other hand, is approximately the middle part of the current Holocene interglacial during which the climate and environment differed from the present day, particularly at northern high latitudes, due to orbital forcing. Both periods provide good opportunities to evaluate climate system responses to large radiative perturbations and to acquire deep insight into present and future climates and environments (Harrison et al., 2015; Masson-Delmotte et al., 2013).

Intensive efforts have been made to investigate LGM and mid-Holocene climatic and environmental changes and underlying dynamic mechanisms through numerous reconstructions and simulations since the 1970s (e.g., CLIMAP Project Members, 1976; COHMAP Members, 1988; MARGO Project Members, 2009). It has been well reconstructed that compared to the present day, the LGM featured a reduction in atmospheric greenhouse gas concentrations, the existence of large continental ice sheets covering northern Europe and North America and associated sea level fall, and prevalent coldness and dryness, while the mid-Holocene exhibited warmer climates at northern midlatitude and high latitude, stronger African and Asian monsoons, and a northward expansion of northern temperate forest relative to today (Jansen et al., 2007; Masson-Delmotte et al., 2013). On the modeling side, the LGM and mid-Holocene are the only two periods that have continued to serve as targets of the Paleoclimate Modeling Intercomparison Project (PMIP) since the 1990s (Joussaume et al., 1999; Taylor et al., 2012). It has been amply documented that climate models can reproduce the direction and broad-scale patterns of LGM and mid-Holocene climate changes as recorded by multiple kinds of paleoclimatic data, indicating their adequate representation of major climatic processes,

although model-data mismatches still exist in certain respects (e.g., Braconnot et al., 2007, 2012; Jansen et al., 2007; Jiang et al., 2012; Kageyama et al., 2006; Liu et al., 2018; Masson-Delmotte et al., 2013; Pinot et al., 1999).

Here we would like to stress that the growing season refers to the period of time in a given year when the climate favors plant growth and is an important factor for describing climate, especially when phenology (the science of naturally recurring events) is concerned. This issue has garnered considerable interest, because the growing season and associated growing degree days respond directly to climatic changes and at the same time also exerts strong control over terrestrial ecosystem functions and in turn an effect on vegetation and atmospheric carbon dioxide and then climate (e.g., Barichivich et al., 2013; Myneni et al., 1997; Peñuelas & Filella, 2001; Reyes-Fox et al., 2014; White et al., 1999). As a key phenological indicator of climate change, the growing season has been widely investigated at varying spatiotemporal scales, particularly from the 20th century onward due to the availability of instrumental records (Linderholm, 2006). Changes in both the timing and length of the growing season over the past few decades, especially its extension and earlier onset, have been well addressed and intrinsically associated with temperature changes at global and continental scales based on a variety of observations and satellite data, which is consistent with understandings of recent global warming (e.g., Barichivich et al., 2013; Menzel & Fabian, 1999; Myneni et al., 1997; Peñuelas & Filella, 2001). It is projected that global warming would lead to a prolongation and intensification of the thermal growing season in the 21st century (e.g., Monier et al., 2016; Ruosteenoja et al., 2016). Besides the modern climate, several studies have been conducted to reconstruct the accumulated temperature sum during the LGM and mid-Holocene growing seasons, as expressed by growing degree days above 5 °C (GDD5), through subfossil-pollen and plant-macrofossil data at regional and global scales (Bartlein et al., 2011; Cheddadi et al., 1997; Tarasov et al., 1999; Wu et al., 2007). Harrison et al. (2014) showed that PMIP models can successfully simulate a decrease in the mean GDD5 at all land grid cells where there are reconstructions (Bartlein et al., 2011) during the LGM and a slight increase during the mid-Holocene, but underestimate the magnitude of reconstructed spatial variability for both periods, particularly for the mid-Holocene. At this stage, however, the geographical distributions of the simulated LGM and mid-Holocene GDD5 changes and their regional comparisons with reconstructions still remain unavailable in the literature. In addition, the LGM and mid-Holocene growing season start and end dates and lengths have thus far not been explicitly investigated from the perspective of numerical simulations.

Based on this context, we present an analysis of the LGM and mid-Holocene growing seasons using daily data drawn from numerical experiments of multiple climate models participating in PMIP, aiming to improve our understanding of phenology and of the integral picture of climate at those periods. We address the following questions: (1) how do growing season-related factors (namely, the first and last days of the growing season, the growing season length [GSL], the growing season temperature, and GDD5 as defined in section 2.2) respond to the LGM and mid-Holocene forcings; and (2) do simulations agree with GDD5 reconstructions at both global and regional scales?

## 2. Data and Methods

### 2.1. Model, Proxy, and Reanalysis Data

Daily model outputs are derived from all available numerical experiments for preindustrial, LGM, and mid-Holocene climates, which were performed by 28, 9, and 24 fully coupled atmosphere-ocean or atmosphere-ocean-vegetation models participating in PMIP Phases 2 (PMIP2) and 3 (PMIP3), respectively. Relative to the preindustrial control run, the LGM climate is driven by changes in the Earth's orbital parameters, ice-sheet extent and associated land-sea mask and topography, and atmospheric concentrations of carbon dioxide, methane, and nitrous oxide. The mid-Holocene external forcings include orbitally induced strengthening of the seasonal contrast in incoming solar radiation at the top of the atmosphere in the northern hemisphere but weakening in the southern hemisphere as well as a reduction in atmospheric methane concentrations. In addition, historical simulations of all available 11 PMIP3 models (Figure S1) for the past ~1.5 centuries with time-varying anthropogenic and natural forcings are used to assess the model performance about the growing-season related variables under the modern climate. Note that the PMIP3 experiments have been integrated in the Coupled Model Intercomparison Project Phase 5 (CMIP5) exercise (Taylor et al., 2012), and they have thus been performed with the exact same

**Table 1**
*Basic Information on the 14 PMIP2 and 14 PMIP3 Models and Their Experiments Included in This Study*

| | | | Length of run analyzed (period in model year) | | |
|---|---|---|---|---|---|
| Model name | Country or union | Atmospheric resolution | Preindustrial | Mid-Holocene | LGM |
| Fourteen coupled atmosphere-ocean or atmosphere-ocean-vegetation (model name shown in italic) models within PMIP2 | | | | | |
| CSIRO-Mk3L-1.1 | Australia | ~5.6° × 3.2°, L18 | 951–1,000 | 951–1,000 | |
| ECBILTCLIO | Netherlands | ~5.6° × ~5.6°, L3 | 2–50 | | 2–50 |
| ECHAM5-MPIOM1 | Germany | 3.75° × ~3.7°, L20 | 2,427–2,476 | 2,428–2,477 | |
| FOAM | USA | 7.5° × ~4.4°, L18 | 300–398 | 300–399 | |
| *FOAM-veg* | USA | 7.5° × ~4.4°, L18 | 300–398 | 300–399 | |
| HadCM3M2 | UK | 3.75° × 2.5°, L19 | 80–99 | | 80–99 |
| *HadCM3M2-veg* | UK | 3.75° × 2.5°, L19 | 80–99 | | 80–99 |
| MIROC3.2 | Japan | ~2.8° × 2.8°, L20 | 1–50 | 1–50 | 1–50 |
| MRI-CGCM2.3.4fa | Japan | ~2.8° × 2.8°, L30 | 2,001–2,100 | 2,001–2,100 | |
| *MRI-CGCM2.3.4fa-veg* | Japan | ~2.8° × 2.8°, L30 | 2,311–2,410 | 2,311–2,410 | |
| MRI-CGCM2.3.4nfa | Japan | ~2.8° × 2.8°, L30 | 2,001–2,100 | 2,001–2,100 | |
| *MRI-CGCM2.3.4nfa-veg* | Japan | ~2.8° × 2.8°, L30 | 2,311–2,410 | 2,311–2,410 | |
| UBRIS-HadCM3M2 | UK | 3.75° × 2.5°, L19 | 0–99 | 0–99 | |
| *UBRIS-HadCM3M2-veg* | UK | 3.75° × 2.5°, L19 | 0–99 | 0–99 | |
| Fourteen coupled atmosphere-ocean or atmosphere-ocean-vegetation (model name shown in italic) models within PMIP3 | | | | | |
| *BCC-CSM1.1* | China | ~2.8° × ~2.8°, L26 | 301–500 | 1–100 | |
| CCSM4 | USA | 1.25° × ~0.9°, L26 | 953–1,108 | 1,269–1,300 | 1,870–1,900 |
| CNRM-CM5 | France | ~1.4° × 1.4°, L31 | 2,500–2,699 | 1,950–2,149 | |
| COSMOS-ASO | Germany | 3.75° × ~3.7°, L19 | 200–399 | | 400–599 |
| CSIRO-Mk3.6.0 | Australia | ~1.875° × ~1.875°, L18 | 301–500 | 1–100 | |
| CSIRO-Mk3L-1-2 | Australia | 5.625° × ~3.18°, L18 | 951–1,000 | 451–500 | |
| EC-EARTH-2-2 | European | 1.125° × 1.125°, L62 | 1,860–1,899 | 1,860–1,899 | |
| *FGOALS-s2* | China | ~2.8° × 3–6°, L26 | 2,151–2,350 | 1–100 | |
| *HadGEM2-CC* | UK | ~1.9° × 1.25°, L60 | 1,900–2,099 | 1,942–1,976 | |
| *HadGEM2-ES* | UK | ~1.9° × 1.25°, L38 | 2,235–2,434 | 2,061–2,162 | |
| *IPSL-CM5A-LR* | France | 3.75° × ~1.9°, L39 | 2,600–2,799 | 2,701–2,800 | |
| *MIROC-ESM* | Japan | ~2.8° × 2.8°, L80 | 2,230–2,429 | 2,330–2,429 | 4,600–4,699 |
| MPI-ESM-P | Germany | 1.875° × ~1.9°, L47 | 2,806–3,005 | 1,850–1,949 | 1,850–1,949 |
| MRI-CGCM3 | Japan | 1.125° × ~1.1°, L48 | 2,151–2,350 | 1,951–2,050 | 2,501–2,699 |

*Note.* A blank area denotes that no data are available. PMIP = Paleoclimate Modelling Intercomparison Project; LGM = last glacial maximum.

model configurations as those used for historical simulations. Basic information on the climate models and data are listed in Table 1. Further details, as well as information on boundary conditions and experimental designs, have been provided by Braconnot et al. (2007) and Taylor et al. (2012) and are available online at http://pmip3.lsce.ipsl.fr/.

The proxy data used for direct comparisons with simulations are reconstructions of the LGM and mid-Holocene GDD5 over ice-free land cells, which are the only direct evidence available for large-scale paleoclimate data-model comparison about thermal growing season so far. These data are obtained on the basis of subfossil-pollen and plant-macrofossil data as derived from sediment profiles using modern analogue, regression, and model-inversion techniques and are quantitatively expressed at 88 grid cells for the LGM and 516 grid cells for the mid-Holocene (Bartlein et al., 2011). In addition, pollen-based quantitative reconstructions of mean annual temperature at 91 and 561 grid cells for the LGM and mid-Holocene (Bartlein et al., 2011), respectively, are indirectly compared to simulations of growing season temperature because of the absence of direct evidence and the close relationship between annual and growing season temperatures (Figure S2).

Three sets of reanalysis data for the period 1979–2005 are used to assess the ability of climate models with historical experiments to simulate the modern growing season-related factors, including the National Center for Environmental Prediction of the Department of Energy Reanalysis II (Kanamitsu et al., 2002) with a horizontal resolution of 1.875° × ~1.9°, the European Centre for Medium-Range Weather Forecasts Reanalysis Interim (ERA-Interim; Dee et al., 2011), and the European Centre for Medium-Range Weather Forecasts pilot reanalysis of the 20th century (ERA-20C; Poli et al., 2013) with a resolution of 2° × ~2°. The

period 1979–2005 is chosen because the reanalysis data are more reliable after 1979 owing to the inclusion of satellite data and because the historical experiment of the models ends in 2005.

Because atmospheric horizontal resolutions differ among models and reanalysis data, all data were interpolated to a regular grid mesh of 2° × 2° using a bilinear interpolation for low-resolution models and an area-weighted interpolation for high-resolution models, given the facts that this grid resolution is a relatively mid-range size of the models and that the reconstructions for data-model comparison are performed at this level. The arithmetic mean of multiple models is calculated with equal weights across the models of concern.

### 2.2. Methods

The definitions of the concerned four growing-season related factors refer to the Joint World Meteorological Organization Commission for Climatology-Climate Variability and Predictability-Joint Commission for Oceanography and Marine Meteorology Expert Team on Climate Change Detection and Indices (http://etccdi.pacificclimate.org/indices.shtml). (1) The GSL is defined as the annual number of days between the first span after 1 January (1 July) of at least six consecutive days with a daily mean near-surface air temperature (2 m) above 5 °C and the first span after 1 July (1 January) of at least six consecutive days with a daily mean temperature below 5 °C in the northern (southern) hemisphere. (2) The first day of the growing season, namely, the growing season start, is defined as the first day of the first occurrence of at least six consecutive days with a daily mean temperature above 5 °C, and (3) the last day of the growing season, namely, the growing season end, is defined as the last day of the first occurrence of at least six consecutive days with a daily mean temperature below 5 °C. (4) The GDD5, an index of growing season warmth, is defined as the sum of the daily mean temperature for days of a year with temperatures higher than a base level of 5 °C, which is regarded as a temperature threshold for woody plants. In addition, the growing season temperature during the LGM (mid-Holocene) is defined as the daily mean temperature averaged over the entire period consisting of both the LGM (mid-Holocene) and preindustrial growing seasons for better addressing differences between the two periods. We use an area-weighted method to calculate area average values, and all our results for LGM and mid-Holocene are anomalies from preindustrial levels.

### 2.3. Evaluation of Climate Models for the Modern Growing Season-Related Factors

Since the ability of climate models in reproducing the modern growing season-related factors is related to the confidence of their results for the LGM and mid-Holocene, historical simulations undertaken by the 11 PMIP3 models are first evaluated against three sets of reanalysis data for 1979–2005. Figure S1 illustrates the range of spatial correlation coefficients, normalized standard deviations, and normalized centered root-mean-square differences of each historical experiment relative to each reanalysis data. Based on 3,710 grid points over global ice-free land areas, these three statistical variables in order are 0.89–0.99, 0.80–1.10, and 0.08–0.46 for the first and last days of the growing season, GSL, GDD5, and growing season temperature, and all spatial correlation coefficients are statistically significant at the 99.9% confidence level. Table S1 further shows that the simulated errors for the five factors are overall small compared with the reanalysis data. Moreover, the arithmetic mean of 11 PMIP3 models reproduces the large-scale geographical distributions of all the five factors in the reanalysis data reasonably well, which highly resembles the spatial patterns as obtained from National Center for Environmental Prediction of the Department of Energy Reanalysis II, although there exists an underestimate in the magnitude of the growing season temperature and GDD5 over Africa and the Arabian and Indian Peninsulas in ERA-Interim and ERA-20C (Figures S3 and S4). As a whole, PMIP3 models reliably capture the main features of the modern spatial pattern and variability of those five growing season-related factors.

## 3. LGM Changes in the Growing Season

### 3.1. Changes in GSL

In comparison to the preindustrial period, all nine models simulated a later start and an earlier end of the growing season averaged over the globe by area-weighting and thus a shorter GSL at the LGM (Figure 1), with the signal being larger than the noise showing by the standard deviation of interannual variability for individual models and by the intermodel standard deviation for all models (Figure S5). The growing season began 9.2 to 18.8 days later and ended 7.0 to 13.1 days earlier at the LGM than at preindustrial, resulting

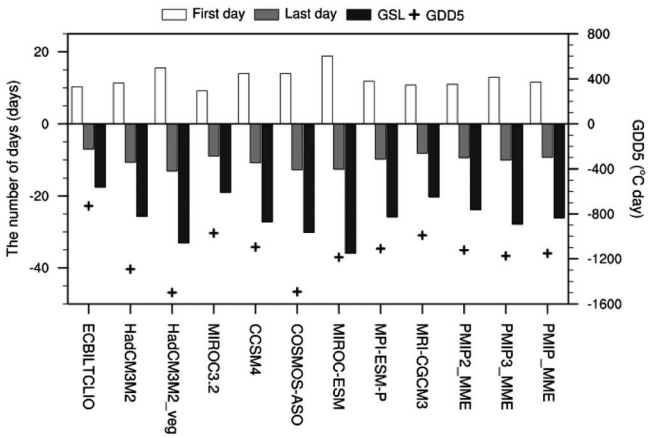


**Figure 1.** Last glacial maximum minus preindustrial levels for globally averaged first and last days of the growing season (units: days), GSL (units: days), and GDD5 (units: °C day) over ice-free land areas for both last glacial maximum and preindustrial periods as derived from nine models and their arithmetic mean. Positive values for the first day indicate a later start of the growing season; negative values for the last day indicate an earlier end of the growing season; and negative values for GSL indicate a shorter growing season. GSL = growing season length; GDD5 = Growing degree days above 5 °C; PMIP = Paleoclimate Modelling Intercomparison Project.

in a GSL reduction of 17.6 to 36.0 days across the nine models. When viewed from the arithmetic mean of individual models, global average GSL at the LGM was 26.1 days shorter than its preindustrial level, owing to a later start of 11.6 days and an earlier end of 9.3 days. Note that here the sum of changes in the start and end dates is not equal to the GSL reduction value. This is because at the LGM there were grid cells for which growing season start and end dates did not exist because at least six consecutive days with a daily mean temperature above 5 °C did not occur, but at the same time GSL was equal to zero at those grid cells; therefore, grid cells used to calculate growing season start and end dates were fewer in number than those for the GSL (Figures 2a–2c).

LGM changes in the growing season start and end dates as well as the GSL were spatially variable over the ice-free land areas (Figures 2a–2c). The growing season start generally became later at midlatitude and high latitude but was little changed at low latitudes relative to the preindustrial. The maximum delay of more than 1 month appeared at midlatitudes of North America and East Europe and in the southwestern region of southern Africa (Figure 2a). A similar spatial pattern and magnitude held true for earlier end dates, as the last day of the growing season shifted to an earlier date at midlatitude and high latitude but changed little at low latitudes (Figure 2b). Both a later start and an earlier end led to a reduction of the GSL at midlatitude and high latitude (Figure 2c). This was particularly noticeable in southern North America close to the Laurentide ice sheet and in central and western Europe close by and downwind from the Fennoscandian ice sheet, where the growing season was shortened by more than 2 months due to generally stronger surface cooling than elsewhere. In contrast, the GSL varied very little at low latitudes because the climatological temperature was high and hence the growing season lasted for all or most of the year in the tropical zone for both the LGM and preindustrial periods (Figure 3a). Comparatively, the nine models agreed qualitatively with one another in terms of the above results for each indicator as denoted by the zonal mean curves obtained from the nine-model arithmetic mean together with the standard deviation of individual models (Figures 2a–2c); model-to-model variability was generally greater at high latitudes than at low latitudes; and the four PMIP2 models performed similarly to the five PMIP3 ones overall (Figure 1).

### 3.2. Changes in Growing Season Temperatures

Consistent with the earlier analysis of the LGM simulations, all nine models reproduced colder than preindustrial climates. The LGM global cooling has been widely attributed to relatively well-defined radiative perturbations stemming from, first, large ice sheets and additionally from lower atmospheric concentrations of greenhouse gases, which were further modified through internal feedbacks in the climate system arising from, for example, snow, sea-ice, dust, vegetation, and water vapor (e.g., Braconnot et al., 2007; Jansen et al., 2007; Masson-Delmotte et al., 2013). At the LGM, global mean temperature differences from the preindustrial level for the ice-free land areas were −5.1 °C for the year in terms of the arithmetic mean of the nine models.

We found that a similar degree of cooling occurred during the growing season, during which daily mean temperatures decreased on average by 3.1 to 6.4 °C for individual models and by 4.6 °C for their arithmetic mean. Figure 2d shows that relative to the preindustrial period, the simulated growing season temperature decreased everywhere, and the magnitude of this decrease varied regionally. At the large scale, this reduction was smaller at low latitudes than at midlatitude and high latitude and was greater close to the Laurentide and Fennoscandian ice sheets due to the cooling effect of large ice sheets together with high albedo levels of sea-ice at high latitudes. An indirect comparison indicates an agreement between simulated growing season temperatures and reconstructed mean annual temperatures at 91 grid cells (Figure 2d; Bartlein et al., 2011), since there is an average decrease of 5.5 °C for the former and 6.1 °C for the latter, and spatial correlation coefficient between each other is 0.54. A further comparison between simulated growing season temperatures and reconstructed mean temperatures of the warmest month at 121 grid cells (Figure S6b;

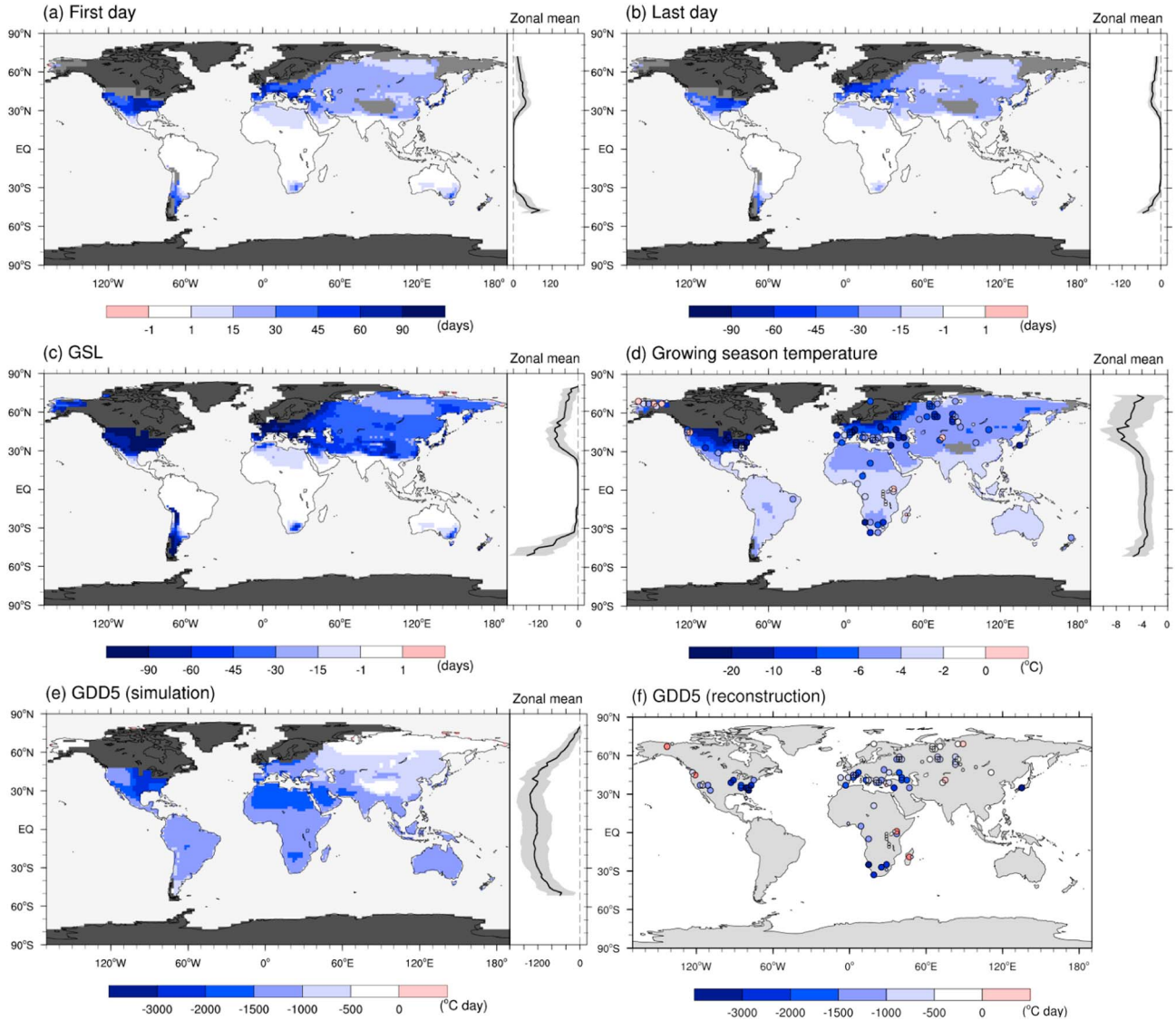


**Figure 2.** LGM minus preindustrial levels for the first and last days of growing season, GSL, growing season temperature, and GDD5 as obtained from the arithmetic mean of nine models, together with GDD5 reconstructions. Dark gray areas denote cells covered by ice sheets at the LGM. In (a) to (e), the right-hand black lines represent the zonal mean changes, and shaded areas represent plus and minus one standard deviation for the models. In (a) and (b), light gray areas on land denote cells with a GSL value of zero at the LGM or preindustrial. In (d) and (f), 91 and 88 circles denote the reconstructed differences in mean annual temperature and GDD5 between LGM and preindustrial respectively, where 77 and 70 large circles indicate points with significant anomalies, respectively, and the remaining small circles indicate anomalies that are not significant (Bartlein et al., 2011). LGM = last glacial maximum; GSL = growing season length; GDD5 = Growing degree days above 5 °C.

Bartlein et al., 2011) gives an identical spatial correlation coefficient of 0.54 between each other, with an agreement in the average decreased signal but a larger change magnitude in simulations (−7.5 °C) than in reconstructions (−5.5 °C).

In addition, daily mean temperature decline remained relatively stable in magnitude throughout the growing season at low latitudes and at austral midlatitudes, but it was more pronounced in the summer than at other times at northern midlatitude and high latitude across the models (Figure 3a).

### 3.3. Changes in GDD5

The LGM GDD5 was also lower than preindustrial levels (Figure 2e), which was due to, first, the cooling and, second, the shortening of the growing season. Negative anomalies were greater at low latitudes than at

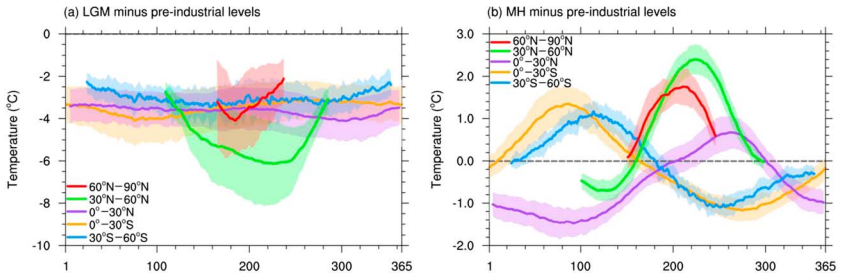


**Figure 3.** (a) LGM and (b) MH minus preindustrial levels for area-averaged daily mean temperature (units: °C) during the common growing season for (a) LGM and preindustrial periods and for (b) MH and preindustrial periods as derived from the arithmetic mean of the (a) 9 and (b) 24 models at different latitudinal zones, respectively, where lightly shaded areas represent plus and minus one standard deviation of the models. For the *x* axis, 1 denotes 1 January (1 July), and 365 denotes 31 December (30 June) in the northern (southern) hemisphere. LGM = last glacial maximum; MH = mid-Holocene.

midlatitude and high latitude due to a longer growing season in the area (Figure 3a). A maximum decline of more than 1,500 °C day occurred in the central and eastern parts of midlatitude North America, in northwestern Europe close to the Fennoscandian ice sheet, and in much of the northern region of northern Africa. A minimum decline of less than 500 °C day appeared in Alaska and neighboring regions, in the Tibetan Plateau, and across much of Eurasia north of ~55°N, where such smaller levels were directly linked to relatively low climatological temperatures and in turn to the short duration of the growing season for both the LGM and preindustrial. The remaining areas experienced a decrease of 500 to 1,500 °C day. At the large scale, similar magnitudes and spatial patterns of GDD5 changes were generally reproduced by the nine models, and model-to-model variability was greater at low latitudes, in concert with greater anomalies, than elsewhere. Globally, GDD5 decreased by 729 to 1,498 °C day (15% to 32%) for individual models and by 1,152 °C day (24%) for their arithmetic mean relative to preindustrial levels (Figure 1), and the signal is much greater than the noise (Figure S5).

When compared to GDD5 reconstructions from subfossil-pollen and plant-macrofossil data at 88 grid cells (Figure 2f, Bartlein et al., 2011), it is clear that the models performed qualitatively well at reproducing decreased signal and spatial pattern of GDD5 changes as suggested by paleoclimatic data at the global scale. Spatial correlation coefficient, normalized standard deviation, and normalized centered root-mean-square difference between simulations and reconstructions at 88 grid cells are 0.54 (statistically significant at the 99.9% confidence level), 0.63, and 0.85, respectively. More specifically, the LGM GDD5 decreased by an area-weighted average of 1,281 °C day for simulations and 1,080 °C day for reconstructions at 88 grid cells, with the same sign of change at 81 out of 88 grid cells and at 64 out of 70 grid cells with significant anomalies (Figures 2e–2f). Where the 70 grid cells with significant anomalies are concerned, the mismatch between simulated GDD5 decrease and reconstructed increase occurs at six sites in Alaska and the Pacific coast of northwestern America, in eastern Africa and Madagascar, and in central Eurasia, and models also underestimate the reconstructed GDD5 decrease at several sites in Japan and southern Africa and around the Mediterranean and the Black Sea. Such mismatch shows an extent of uncertainty in proxy data partly due to their relatively sparse spatial coverage, particularly in the southern hemisphere where the reconstructions at only 14 grid cells all locate in southern Africa (Figure 2f), and also in climate models probably arising from their incorrect or missing representation of important internal feedbacks such as vegetation and dust feedbacks (Hargreaves et al., 2013; Masson-Delmotte et al., 2013). However, of importance is that both simulation and reconstruction uncertainties are small relative to the magnitude of global mean difference (Figures S5 and S7), and simulations agree better with reconstructions in the northern hemisphere than in southern Africa of the southern hemisphere (Figure S8a).

## 4. Mid-Holocene Changes in the Growing Season

### 4.1. Changes in GSL

The mid-Holocene global average growing season start and end dates and length were similar to preindustrial conditions. The start and end dates varied only by −1.3 to 3.0 days and by −1.0 to 2.6 days, respectively, while the length varied by −3.9 to 3.4 days across the 24 individual models (Figure 4). All these values lie

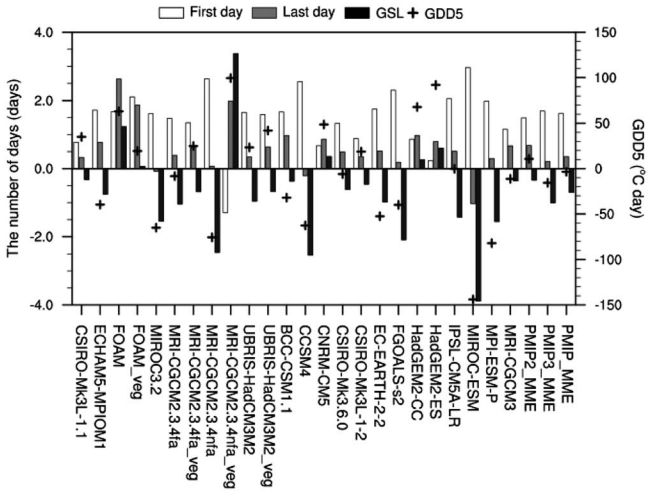


**Figure 4.** Mid-Holocene minus preindustrial levels for globally averaged first and last days of growing season (units: days), GSL (units: days), and GDD5 (units: °C day) as derived from 24 models and their arithmetic mean. For the former three factors, positive values indicate a later onset or end of the growing season or a longer one, and negative values indicate an earlier onset or end of the growing season or a shorter one. GSL = growing season length; GDD5 = Growing degree days above 5 °C; PMIP = Paleoclimate Modelling Intercomparison Project.

within the scope of the standard deviation of interannual variability for the mid-Holocene and preindustrial periods for individual models and of the intermodel standard deviation for all models (Figure S9), indicating a smaller signal than the noise and a degree of the model uncertainty. In general, most models reproduced a decrease in the length and later start and end dates, namely, a shift in the whole growing season toward autumn, which was a first-order response to orbital forcing. As far as the arithmetic mean of 24 models is concerned, the global average GSL decreased insignificantly by 0.7 days due to a greater delay in the start dates than in the end dates.

Figure 5a shows that the mid-Holocene growing season generally began later than the preindustrial counterpart at approximately 20–60°N but earlier north of ~60°N, and few changes occurred in other areas except for in the southernmost part of southern Africa where an earlier start appeared. End dates were generally earlier at approximately 20–40°N and in the southernmost part of southern Africa but later north of ~40°N (Figure 5b). Both the start and end dates of the growing season varied very little at low latitudes due to high climatological temperatures that gave rise to almost full-year growing seasons for both the mid-Holocene and preindustrial periods. Taken together, the mid-Holocene growing season prolonged north of ~50°N, shortened across much of 20–50°N, and reflected preindustrial levels at low latitudes (Figure 5c). At the large scale, 24 individual models reproduced comparable changes in patterns and magnitudes of mid-Holocene growing season start and end dates and lengths, though we found a degree of uncertainty as indicated by the zonal mean curves derived from the 24-model arithmetic mean and the accompanying plus and minus one standard deviation of individual models (Figures 5a–5c). Eleven PMIP2 models also performed similarly to the 13 PMIP3 ones as a whole (Figure 4).

Vegetation feedback has been regarded as an important process in the mid-Holocene climate system (e.g., Ganopolski et al., 1998; Kutzbach et al., 1996). Considering the relationship between the growing season and vegetation, we performed a preliminary analysis of vegetation feedback using simulations from four pairs of climate models within PMIP2, namely, FOAM, MRI-CGCM2.3.4fa, MRI-CGCM2.3.4nfa, UBRIS-HadCM3M2, and their atmosphere-ocean-vegetation model counterparts (Table 1). Note that each pair of the models shares the same atmosphere-ocean model component, and a dynamic global vegetation model is the only difference between them. Figure 4 indicates that interactive vegetation led to additional small changes in GSL during the mid-Holocene. Compared to the values from MRI-CGCM2.3.4fa, MRI-CGCM2.3.4nfa, and UBRIS-HadCM3M2 (FOAM), the growing season derived from their atmosphere-ocean-vegetation model counterparts was prolonged (shortened) globally due to an earlier (later) start and a later (earlier) end. More specifically, although statistically insignificant, the mid-Holocene changes in growing season start and end dates and length due to the vegetation effect were −0.1, 0.3, and 0.4 days from the MRI-CGCM2.3.4fa pair; −3.9, 1.9, and 5.8 days from the MRI-CGCM2.3.4nfa pair; −0.1, 0.3, and 0.3 days from the UBRIS-HadCM3M2 pair; but were 0.4, −0.8, and −1.2 days from the FOAM pair, respectively. Note that there are also six atmosphere-ocean-vegetation models within PMIP3 (Table 1). However, the absence of simulations from their atmosphere-ocean model counterparts prevents a further investigation on the pure vegetation feedback at this stage.

### 4.2. Changes in Growing Season Temperatures

It has been well documented that the most important forcing for the mid-Holocene lies in the orbitally induced stronger than preindustrial seasonality of incoming solar radiation at the top of the atmosphere in the northern hemisphere but weaker one in the southern hemisphere due to precessional variations (Berger, 1978; Jansen et al., 2007; Masson-Delmotte et al., 2013). More specifically, more insolation was generally received from mid-May to October in the northern hemisphere and from July to mid-December in the southern hemisphere, but less was received for other times (Figure S10). In response to this orbital forcing and a slight reduction in atmospheric methane concentrations, the mid-Holocene global mean

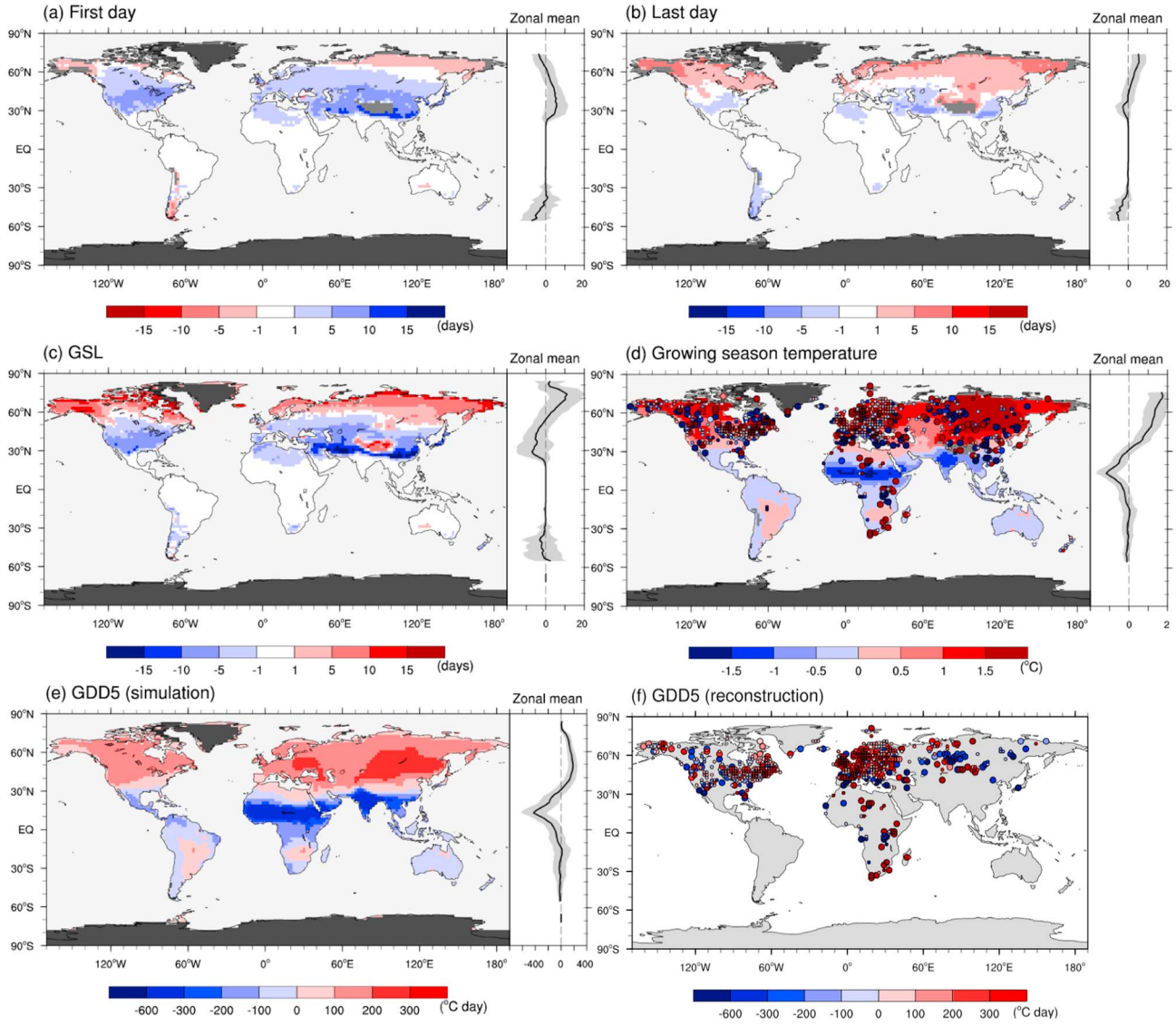


**Figure 5.** Mid-Holocene minus preindustrial levels for the first and last days of growing season, GSL, growing season temperature, and GDD5 as obtained from the arithmetic mean of 24 models, together with GDD5 reconstructions. Dark gray areas denote cells covered by ice sheets at the preindustrial. In (a) to (e), the right-hand black lines represent the zonal mean changes, and shaded areas represent plus and minus one standard deviation for the models. In (a) and (b), light gray areas on land denote cells with a GSL value of zero at the mid-Holocene or preindustrial. In (d) and (f), 561 and 516 circles denote the reconstructed differences in mean annual temperature and GDD5 between mid-Holocene and preindustrial, respectively, where 248 and 288 large circles indicate points with significant anomalies, respectively, and the remaining small circles indicate anomalies that are not significant (Bartlein et al., 2011). GSL = growing season length; GDD5 = Growing degree days above 5 °C.

temperature over ice-free land varied by −0.1 °C for the year, by −0.4 °C for December to February, by −0.5 °C for March to May, by 0.6 °C for June to August, and by 0.03 °C for September to November relative to the preindustrial state according to the 24-model arithmetic mean. Note that these anomalies generally followed insolation variations in the northern hemisphere, where most of the global ice-free land is located. Since there is so much more land area in the northern hemisphere than in the southern hemisphere, the global average is being skewed toward the northern hemisphere.

For the growing season, global mean temperatures varied from −0.3 to 0.9 °C for individual models and increased by 0.2 °C for their arithmetic mean. Geographically, the mid-Holocene growing season temperature increased and amplified northward north of ~30°N, while a decrease occurred at 10°S–30°N, particularly in tropical Africa at approximately 10–20°N and in northern India (Figure 5d). Few changes appeared south of

~10°S. The general increase at northern midlatitude and high latitude and decrease in the tropics are direct consequences of the mid-Holocene orbitally induced changes in annual insolation values (Figure S10). Comparatively, the simulated zonal pattern of growing season temperature anomalies relative to the preindustrial period differs from a large spatial variability of both reconstructed mean annual temperatures at 561 grid cells (Figure 5d) and reconstructed mean temperatures of the warmest month at 599 grid cells (Figure S11b), and the anomalies are generally smaller for the simulations than for the reconstructions.

In addition, mid-Holocene daily temperature differences from preindustrial levels through the growing season varied considerably over time (Figure 3b). Area-averaged daily temperature anomaly was positive for most of the growing season at 60–90°N and 30–60°N, with the most significant warming trends occurring during the summer, while negative patterns were characteristic at northern low latitudes except from July to October. An increase only occurred in early July to mid-January and from August to January in latitudinal zones of 0–30°S and 30–60°S, respectively.

### 4.3. Changes in GDD5

Mid-Holocene GDD5 differed from preindustrial levels in a zonal distribution (Figure 5e). The GDD5 increased at midlatitude and high latitude north of ~30°N but decreased at northern low latitudes, while negative anomalies were registered in most austral land areas except for in southeastern South America and in the central-southern part of southern Africa, where a warmer than preindustrial growing season (Figure 5d) gave rise to an increase in GDD5. Such a spatial pattern is similar to that of the growing season temperature changes (Figures 5d–5e) and is a response to orbital forcing (Figure S10). The maximum GDD5 increase of ~200 °C day occurred at northern midlatitude and high latitude, owing first to increased temperatures and second to a longer growing season. Tropical Africa at approximately 5–20°N and India experienced a maximum reduction of −687 to −300 °C day due to a maximum drop in growing season temperatures (Figure 5d). Comparatively, the scatter of zonal mean GDD5 changes, as shown in the shaded areas of the right-hand panel in Figure 5e, was small among individual models. Averaged over the globe, the mid-Holocene GDD5 varied by −144 to 99 °C day (−3.2% to 2.9%) for individual models and averaged at −4 °C day (−0.1%) for all models relative to preindustrial levels (Figure 4), and the signal is smaller than the noise (Figure S9). The vegetation feedback also led to additional GDD5 changes during the mid-Holocene. Globally, it induced an insignificant increase of GDD5 by 33, 175, and 19 °C day from the MRI-CGCM2.3.4fa, MRI-CGCM2.3.4nfa, and UBRIS-HadCM3M2 pair, respectively, but a decrease of 44 °C day from the FOAM pair (Figure 4).

Mid-Holocene changes in GDD5 were reconstructed at 516 land grid cells using subfossil-pollen and plant-macrofossil data (Figure 5f, Bartlein et al., 2011). At the regional scale, GDD5 increased over northern Europe but decreased over most of southern Europe around the Mediterranean, and this was supported by previous reconstructions based on different pollen data sets through a modern analogue approach constrained by lake-level data (Cheddadi et al., 1997), through a climatic calibration based on the scores of plant functional types (Tarasov et al., 1999), and via inverse modeling (Wu et al., 2007). The rest of midlatitude and high-latitude Eurasia featured a tripartite latitudinal pattern with a moderate increase along the Arctic coast, a deficit in the zone from ca. 45–65°N, and an increase in the continental interior. In North America, positive anomalies occurred along the northern coast and along much of the northeastern part of the continent, while negative ones occurred in the American Southwest, in the southern part of the continent, and in the interior of northwestern Canada. Such reductions were characteristic in equatorial Africa and at several sites in the western Sahara, while the opposite held for the surrounding zone including the eastern Sahara, eastern Africa, and southern Africa. Thus, the local pattern of GDD5 changes in some regions at midlatitude and high latitude north of ~40°N is different between simulations and reconstructions (Figures 5e–5f), although the zonal mean changes over these areas are generally consistent (Figure S8b). When all 516 grid cells are considered, the mid-Holocene GDD5 increased by an area-weighted average of 102 °C day for simulations and 116 °C day for reconstructions, with a higher uncertainty for the latter than for the former (Figure S7). Simulations agree in sign with reconstructions at 325 out of 516 grid cells and at 192 out of 288 grid cells with significant anomalies, which is indicative of an ability of the models in reproducing the direction of large-scale GDD5 changes, particularly in eastern North America and central and northern Europe which have more than half of the 516 grid cells (Figures 5e–5f). However, it is also noted that simulations are generally opposite to reconstructions in southern Europe, at ca. 45–65°N in Eurasia, in the American Southwest, and in eastern

Africa. The simulated magnitude is remarkably smaller than reconstructed, because the normalized standard deviation between simulations and reconstructions at 516 grid cells is only 0.16. Simulated changes in zonal mean GDD5 are clearly smaller than reconstructed at 40°S–40°N (Figure S8b). In other words, the models underestimated the reconstructed magnitude of mid-Holocene GDD5 changes, just as they did for the aforementioned mid-Holocene growing season temperature. This is probably due to their insufficient sensitivity to external perturbations given the fact that the mid-Holocene globally and annually averaged forcing anomaly is very weak relative to the modern period, their underestimation of internal natural variability, and their incorrect or missing representation of important feedbacks among the components of the climate system arising, for example, from land surface and carbon cycle (Braconnot et al., 2012; Hargreaves et al., 2013; Harrison et al., 2014). For example, our preliminary analysis shows that the vegetation feedback gave rise to an increase in GDD5 globally from three out of four pairs of PMIP2 models with and without vegetation effects, which narrows the aforementioned model-data mismatch for the mid-Holocene GDD5. However, the global vegetation model component is still missing in half of the PMIP2/3 models. Therefore, both climate models and the numerical experiment design need to be improved in future studies. On the other hand, the proxy data are very sparse in spatial resolution at northern low latitudes and in the southern hemisphere, which calls for more reconstructions over there as well. For instance, the proxy data in the southern hemisphere all locate in southern Africa at 22 grid cells with an increase at 12 grid cells but a decrease at 10 grid cells (Figure 5f), showing a large degree of uncertainty.

## 5. Conclusion and Discussion

In this study, the LGM and mid-Holocene thermal growing seasons were examined over ice-free land using the daily output of PMIP2/3 experiments undertaken by 9 and 24 climate models, respectively. Our primary conclusions are as follows.

Compared to the preindustrial growing season, LGM cooling led to a later start date, an earlier end date, and a 26.1-day decrease of the length averaged across the nine models. These changes mainly occurred at midlatitude and high latitude where greater drops in temperature occurred and were small at low latitudes where the growing season almost occurred year-round. Daily temperature decrease was generally stable over time at low latitudes, was more pronounced during the summer than during other periods at midlatitude and high latitude, and averaged at −4.6 °C for the growing season. Growing season shortening and cooling gave rise to a 24% reduction in GDD5, which agrees qualitatively well with reconstructions at 88 grid cells.

The mid-Holocene growing season remained nearly identical to the preindustrial state when analyzed at the global scale. GSL, temperature, and GDD5 varied on average by only −0.7 days, 0.2 °C, and − 0.1%, respectively. In response to mid-Holocene orbital forcing, the growing season was longer at northern high latitudes, was shorter in much of the 20–50°N area, and remained almost unchanged in other areas. The growing season warmed north of ~30°N, cooled at approximately 10°S–30°N, and varied slightly south of ~10°S, while a similar pattern held for GDD5. Globally, the GDD5 simulations were qualitatively consistent with, but were weaker than, the majority of reconstructions. Mid-Holocene daily temperature differences from preindustrial levels through the growing season varied considerably over time and showed the highest levels of warming during the summer at northern midlatitude and high latitude.

In addition, it should be noted that the growing season is one of the key factors to affect vegetation growth and distribution (e.g., Linderholm, 2006; Martin, 1993). At the large scale, the reconstructed LGM vegetation differs from the modern one and is characterized mainly by a southward displacement and reductions in forest area over midlatitude and high-latitude northern continents, an expansion of tundra over the northern continents, a fragmentation of boreal evergreen forests and temperate deciduous forests, and reductions in tropical rain forest and tropical seasonal forest in Africa (e.g., Bigelow et al., 2003; Prentice et al., 2000), all of which may have some relationship with the simulated decrease in GSL, GDD5, and growing season temperature for that time (Figures 2c–2e). On the other hand, some connections may also exist between the mid-Holocene changes in the simulated growing season and reconstructed vegetation distribution. Pollen-based reconstructions and macrofossils indicate a northward expansion of forest at the expense of tundra at northern midlatitude to high latitude during the mid-Holocene relative to the modern period (e.g., Bigelow et al., 2003; Kaplan et al., 2003; MacDonald et al., 2000; Prentice et al., 2000), which may be related to the aforementioned increase in GSL, growing season

temperature, and GDD5 (Figures 5c–5e). The increase in the mid-Holocene growing season temperature and GDD5 over northern China (Figures 5d–5e) may also associate with a northward shift of the forest biomes in eastern China as reconstructed from pollen data for that time (Ni et al., 2010; Yu et al., 2000). However, Jolly and Haxeltine (1997) demonstrated the impact of changes in both atmospheric carbon dioxide concentration and climate on vegetation distribution from a terrestrial biosphere model. They proposed that the lower LGM atmospheric carbon dioxide concentration alone could explain the observed reduction of tropical African montane forest, even with the present temperature and precipitation values. Recently, Izumi and Bartlein (2016) also implied that if there was no change between the LGM and present-day climate, the LGM vegetation over North America would still appear direr than present simply due to lower atmospheric carbon dioxide concentration. Therefore, the interaction between climate and vegetation is complicated, which calls for further investigation by performing special experiments using vegetation models. Finally, we would like to stress that because the climate changes during the LGM and mid-Holocene were response to different boundary conditions (ice-sheets, greenhouse gases, and orbital parameters) from the present day and internal feedbacks in the climate system (snow, sea-ice, dust, land surface, carbon cycle, and water vapor), further experiments and analyses are required to disentangle the contribution of each forcing and feedback to the growing season changes described here.

**Acknowledgments**

We sincerely thank the two anonymous reviewers for their insightful comments and suggestions to improve this manuscript. We also acknowledge the climate modeling groups (listed in Table 1) for producing and sharing their model outputs. All the data used here are listed in the references or archived in the PMIP3 repository (online at http://pmip3.lsce.ipsl.fr/). This work was supported by the National Natural Science Foundation of China (41625018), the Strategic Priority Research Program of Chinese Academy of Sciences (XDA20070103), and the National Natural Science Foundation of China (41421004).

## References

Barichivich, J., Briffa, K. R., Myneni, R. B., Osborn, T. J., Melvin, T. M., Ciais, P., et al. (2013). Large-scale variations in the vegetation growing season and annual cycle of atmospheric $CO_2$ at high northern latitudes from 1950 to 2011. *Global Change Biology*, *19*, 3167–3183. https://doi.org/10.1111/gcb.12283

Bartlein, P. J., Harrison, S. P., Brewer, S., Connor, S., Davis, B. A. S., Gajewski, K., et al. (2011). Pollen-based continental climate reconstructions at 6 and 21 ka: A global synthesis. *Climate Dynamics*, *37*, 775–802. https://doi.org/10.1007/s00382-010-0904-1

Berger, A. L. (1978). Long-term variations of daily insolation and Quaternary climatic changes. *Journal of the Atmospheric Sciences*, *35*, 2362–2367. https://doi.org/10.1175/1520-0469(1978)035<2362:LTVODI>2.0.CO;2

Bigelow, N. H., Brubakerm, L. B., Edwards, M. E., Harrison, S. P., Prentice, I. C., Anderson, P. M., et al. (2003). Climate change and Arctic ecosystems: 1. Vegetation changes north of 55°N between the last glacial maximum, mid-Holocene, and present. *Journal of Geophysical Research*, *108*(D19), 8170. https://doi.org/10.1029/2002JD002558

Braconnot, P., Harrison, S. P., Kageyama, M., Bartlein, P. J., Masson-Delmotte, V., Abe-Ouchi, A., et al. (2012). Evaluation of climate models using palaeoclimatic data. *Nature Climate Change*, *2*, 417–424. https://doi.org/10.1038/nclimate1456

Braconnot, P., Otto-Bliesner, B., Harrison, S., Joussaume, S., Peterchmitt, J.-Y., Abe-Ouchi, A., et al. (2007). Results of PMIP2 coupled simulations of the mid-Holocene and last glacial maximum – Part 1: Experiments and large-scale features. *Climate of the Past*, *3*, 261–277. https://doi.org/10.5194/cp-3-261-2007

Cheddadi, R., Yu, G., Guiot, J., Harrison, S. P., & Prentice, I. C. (1997). The climate of Europe 6000 years ago. *Climate Dynamics*, *13*, 1–9.

CLIMAP Project Members (1976). The surface of the ice-age Earth. *Science*, *191*, 1131–1137. https://doi.org/10.1126/science.191.4232.1131

COHMAP Members (1988). Climatic changes of the last 18,000 years: Observations and model simulations. *Science*, *241*, 1043–1052. https://doi.org/10.1126/science.241.4869.1043

Dee, D. P., Uppala, S. M., Simmons, A. J., Berrisford, P., Poli, P., Kobayashi, S., et al. (2011). The ERA-Interim reanalysis: Configuration and performance of the data assimilation system. *Quarterly Journal of the Royal Meteorological Society*, *137*, 553–597. https://doi.org/10.1002/qj.828

Ganopolski, A., Kubatzki, C., Claussen, M., Brovkin, V., & Petoukhov, V. (1998). The influence of vegetation–atmosphere–ocean interaction on climate during the mid-Holocene. *Science*, *280*, 1916–1919. https://doi.org/10.1126/science.280.5371.1916

Hargreaves, J. C., Annan, J. D., Ohgaito, R., Paul, A., & Abe-Ouchi, A. (2013). Skill and reliability of climate model ensembles at the last glacial maximum and mid-Holocene. *Climate of the Past*, *9*, 811–823. https://doi.org/10.5194/cp-9-811-2013

Harrison, S. P., Bartlein, P. J., Brewer, S., Prentice, I. C., Boyd, M., Hessler, I., et al. (2014). Climate model benchmarking with glacial and mid-Holocene climates. *Climate Dynamics*, *43*, 671–688. https://doi.org/10.1007/s00382-013-1922-6

Harrison, S. P., Bartlein, P. J., Izumi, K., Li, G., Annan, J., Hargreaves, J., et al. (2015). Evaluation of CMIP5 palaeo-simulations to improve climate projections. *Nature Climate Change*, *5*, 735–743. https://doi.org/10.1038/nclimate2649

Izumi, K., & Bartlein, P. J. (2016). North American paleoclimate reconstructions for the last glacial maximum using an inverse modeling through iterative forward modeling approach applied to pollen data. *Geophysical Research Letters*, *43*, 10965–10972. https://doi.org/10.1002/2016GL070152

Jansen, E., Overpeck, J., Briffa, K., Duplesey, J., Joos, F., Masson-Delmotte, V., et al. (2007). Palaeoclimate. In S. Solomon, D. Qin, M. Manning, Z. Chen, M. Marquis, K. B. Averyt, et al. (Eds.), *Climate change 2007: The physical science basis. Contribution of working group I to the fourth assessment report of the intergovernmental panel on climate change* (pp. 433–497). Cambridge, United Kingdom and New York, NY, USA: Cambridge University Press.

Jiang, D., Lang, X., Tian, Z., & Wang, T. (2012). Considerable model–data mismatch in temperature over China during the mid-Holocene: Results of PMIP simulations. *Journal of Climate*, *25*, 4135–4153. https://doi.org/10.1175/JCLI-D-11-00231.1

Jolly, D., & Haxeltine, A. (1997). Effect of low glacial atmospheric $CO_2$ on tropical African montane vegetation. *Science*, *276*, 786–788. https://doi.org/10.1126/science.276.5313.786

Joussaume, S., Taylor, K. E., Braconnot, P., Mitchell, J. F. B., Kutzbach, J. E., Harrison, S. P., et al. (1999). Monsoon changes for 6000 years ago: Results of 18 simulations from the Paleoclimate Modeling Intercomparison Project (PMIP). *Geophysical Research Letters*, *26*, 859–862. https://doi.org/10.1029/1999GL900126

Kageyama, M., Laîné, A., Abe-Ouchi, A., Braconnot, P., Cortijo, E., Crucifix, M., et al. (2006). Last glacial maximum temperatures over the North Atlantic, Europe and western Siberia: A comparison between PMIP models, MARGO sea-surface temperatures and pollen-based reconstructions. *Quaternary Science Reviews*, *25*, 2082–2102. https://doi.org/10.1016/j.quascirev.2006.02.010

Kanamitsu, M., Ebisuzaki, W., Woollen, J., Yang, S.-K., Hnilo, J. J., Fiorino, M., et al. (2002). NCEP–DOE AMIP-II reanalysis (R-2). *Bulletin of the American Meteorological Society*, *83*, 1631–1644. https://doi.org/10.1175/BAMS-83-11-1631

Kaplan, J. O., Bigelow, N. H., Prentice, I. C., Harrison, S. P., Bartlein, P. J., Christensen, T. R., et al. (2003). Climate change and Arctic ecosystems: 2. Modeling, paleodata-model comparisons, and future projections. *Journal of Geophysical Research*, *108*(D19), 8171. https://doi.org/10.1029/2002JD002559

Kutzbach, J., Bonan, G., Foley, J., & Harrison, S. P. (1996). Vegetation and soil feedbacks on the response of the African monsoon to orbital forcing in the early to middle Holocene. *Nature*, *384*, 623–626. https://doi.org/10.1038/384623a0

Linderholm, H. W. (2006). Growing season changes in the last century. *Agricultural and Forest Meteorology*, *137*, 1–14. https://doi.org/10.1016/j.agrformet.2006.03.006

Liu, S., Jiang, D., & Lang, X. (2018). A multi-model analysis of moisture changes during the last glacial maximum. *Quaternary Science Reviews*, *191*, 363–377. https://doi.org/10.1016/j.quascirev.2018.05.029

MacDonald, G. M., Velichko, A. A., Kremenetski, C. V., Borisova, O. K., Goleva, A. A., Andreev, A. A., et al. (2000). Holocene treeline history and climate change across northern Eurasia. *Quaternary Research*, *53*, 302–311. https://doi.org/10.1006/qres.1999.2123

MARGO Project Members (2009). Constraints on the magnitude and patterns of ocean cooling at the last glacial maximum. *Nature Geoscience*, *2*, 127–132. https://doi.org/10.1038/ngeo411

Martin, P. (1993). Vegetation responses and feedbacks to climate: A review of models and processes. *Climate Dynamics*, *8*, 201–210. https://doi.org/10.1007/BF00207966

Masson-Delmotte, V., Schulz, M., Abe-Ouchi, A., Beer, J., Ganopolski, A., González Rouco, J. F., et al. (2013). Information from paleoclimate archives. In T. F. Stocker, D. Qin, G. K. Plattner, M. Tignor, S. K. Allen, J. Boschung, et al. (Eds.), *Climate change 2013: The physical science basis. Contribution of working group I to the fifth assessment report of the intergovernmental panel on climate change* (pp. 383–464). Cambridge, United Kingdom and New York, NY, USA: Cambridge University Press.

Menzel, A., & Fabian, P. (1999). Growing season extended in Europe. *Nature*, *397*, 659. https://doi.org/10.1038/17709

Monier, E., Xu, L., & Snyder, R. (2016). Uncertainty in future agro-climate projections in the United States and benefits of greenhouse gas mitigation. *Environmental Research Letters*, *11*, 11. https://doi.org/10.1088/1748-9326/11/5/055001

Myneni, R. B., Keeling, C. D., Tucker, C. J., Asrar, G., & Nemani, R. R. (1997). Increased plant growth in the northern high latitudes from 1981 to 1991. *Nature*, *386*, 698–702. https://doi.org/10.1038/386698a0

Ni, J., Yu, G., Harrison, S. P., & Prentice, I. C. (2010). Palaeovegetation in China during the late Quaternary: Biome reconstructions based on a global scheme of plant functional types. *Palaeogeography, Palaeoclimatology, Palaeoecology*, *289*, 44–61. https://doi.org/10.1016/j.palaeo.2010.02.008

Peñuelas, J., & Filella, I. (2001). Responses to a warming world. *Science*, *294*, 793–795. https://doi.org/10.1126/science.1066860

Pinot, S., Ramstein, G., Harrison, S. P., Prentice, I. C., Guiot, J., Stute, M., et al. (1999). Tropical paleoclimates at the last glacial maximum: Comparison of Paleoclimate Modeling Intercomparison Project (PMIP) simulations and paleodata. *Climate Dynamics*, *15*, 857–874. https://doi.org/10.1007/s003820050318

Poli, P., Hersbach, H., Tan, D., Dee, D., Thépaut, J.-N., Simmons, A., et al. (2013). The data assimilation system and initial performance evaluation of the ECMWF pilot reanalysis of the 20th-century assimilating surface observations only (ERA-20C). ERA Report Series No. 14, ECMWF Technical Report, UK, 1–59.

Prentice, I. C., Jolly, D., & BIOME 6000 participants (2000). Mid-Holocene and glacial-maximum vegetation geography of the northern continents and Africa. *Journal of Biogeography*, *27*, 507–519. https://doi.org/10.1046/j.1365-2699.2000.00425.x

Reyes-Fox, M., Steltzer, H., Trlica, M. J., McMaster, G. S., Andales, A. A., LeCain, D. R., et al. (2014). Elevated $CO_2$ further lengthens growing season under warming conditions. *Nature*, *510*, 259–262. https://doi.org/10.1038/nature13207

Ruosteenoja, K., Räisänen, J., Venäläinen, A., & Kämäräinen, M. (2016). Projections for the duration and degree days of the thermal growing season in Europe derived from CMIP5 model output. *International Journal of Climatology*, *36*, 3039–3055. https://doi.org/10.1002/joc.4535

Tarasov, P. E., Guiot, J., Cheddadi, R., Andreev, A. A., Bezusko, L. G., Blyakharchuk, T. A., et al. (1999). Climate in northern Eurasia 6000 years ago reconstructed from pollen data. *Earth and Planetary Science Letters*, *171*, 635–645. https://doi.org/10.1016/S0012-821X(99)00171-5

Taylor, K. E., Stouffer, R. J., & Meehl, G. A. (2012). An overview of CMIP5 and the experiment design. *Bulletin of the American Meteorological Society*, *93*, 485–498. https://doi.org/10.1175/BAMS-D-11-00094.1

White, M. A., Running, S. W., & Thornton, P. E. (1999). The impact of growing-season length variability on carbon assimilation and evapotranspiration over 88 years in the eastern US deciduous forest. *International Journal of Biometeorology*, *42*, 139–145. https://doi.org/10.1007/s004840050097

Wu, H., Guiot, J., Brewer, S., & Guo, Z. (2007). Climatic changes in Eurasia and Africa at the last glacial maximum and mid-Holocene: Reconstruction from pollen data using inverse vegetation modelling. *Climate Dynamics*, *29*, 211–229. https://doi.org/10.1007/s00382-007-0231-3

Yu, G., Chen, X., Ni, J., Cheddadi, R., Guiot, J., Han, H., et al. (2000). Palaeovegetation of China: A pollen data-based synthesis for the mid-Holocene and last glacial maximum. *Journal of Biogeography*, *27*, 635–664. https://doi.org/10.1046/j.1365-2699.2000.00431.x